ARTICLES

Resolution of Three Fluorescence Components in the Spectra of all-*trans*-1,6-Diphenyl-1,3,5-hexatriene under Isopolarizability Conditions[1]

Andrzej M. Turek,*,† Govindarajan Krishnamoorthy, Donald F. Sears, Jr., Ivelitza Garcia, Olga Dmitrenko,‡ and Jack Saltiel*

Department of Chemistry and Biochemistry, Florida State University, Tallahassee, Florida 32306-4390

Received: October 20, 2004

all-*trans*-1,6-Diphenyl-1,3,5-hexatriene (DPH) fluorescence in solution consists of emissions from the S_1 (2^1A_g) and S_2 (1^1B_u) states of the s-trans,s-trans conformer (*s*-*t*-DPH) and emission from the S_1 state of the s-cis,s-trans conformer (*s*-*c*-DPH). The contribution of *s*-*c*-DPH fluorescence increases upon excitation at longer wavelengths, and both minor emissions, *s*-*c*-DPH and 1^1B_u *s*-*t*-DPH fluorescence, contribute more at higher temperatures (*T*s). Resolution of a spectrothermal matrix of DPH fluorescence spectra by principal component analysis with self-modeling (PCA-SM) is hampered by *T*-dependent changes in the spectra of the individual components. We avoided differential polarizability-dependent spectral shifts by measuring the spectra in *n*-alkanes (C_n, C_8 to C_{16} with *n* even) at *T* values selected to keep the index of refraction constant, hence under isopolarizability conditions. Compensation of the spectra for *T*-induced broadening allowed resolution of the spectral matrix into its three components. The optimum van't Hoff plot gives $\Delta H = 2.83$ kcal/mol for *s*-*c*-DPH/*s*-*t*-DPH equilibration, somewhat smaller than the 3.4 kcal/mol calculated value, and the optimum Boltzmann distribution law plot gives $\Delta E_{ab} = 4.09$ kcal/mol for $1^1B_u/2^1A_g$ equilibration. The 1^1B_u fluorescence spectrum bears mirror-image symmetry with the DPH absorption spectrum, and the energy gap, 1431 cm^{-1}, is consistent with the 1615 cm^{-1} difference between the lowest energy bands in the 1^1B_u and 2^1A_g fluorescence spectra. The results give $V_{ab} = 198 \pm 12$ cm^{-1} for the vibronic matrix coupling element between the 2^1A_g and 1^1B_u states. Fluorescence quantum yields and lifetimes under isopolarizability conditions reveal an increase in the effective radiative rate constant of *s*-*t*-DPH with increasing *T*.

Introduction

The photochemistry and photophysics of α,ω-diphenylpolyenes have been under scrutiny because these molecules are considered to be models for the retinyl polyenes that are related to vitamin A and the visual pigments.[2−5] Excited states of planar all-*trans*-diphenylpolyenes are designated as n^1A_g or n^1B_u based on symmetry. Hudson and Kohler first recognized that for the all-s-trans conformer of planar all-*trans*-diphenyloctatetraene (DPO) the 1^1B_u state, which is responsible for the strong longest wavelength vibronic bands in the electronic absorption spectrum, is not the lowest-energy excited singlet state that is observed in fluorescence.[6] The fluorescence was assigned to the doubly excited 2^1A_g state, which was identified as the lowest excited state. In an accompanying publication, Karplus and Shulten showed that the inclusion of doubly excited configurations in the configuration interaction scheme is crucial for predicting the proper ordering of excited singlet states in polyene hydrocarbons.[7,8] Advanced theoretical approaches such as time-dependent density functional theory (TDDFT) that do not include doubly excited states fail to predict the correct S_2/S_1 order both in the parent polyenes[9,10] and in the α,ω-diphenylpolyenes.[11] "Dressed" TDDFT includes doubly excited states and predicts the correct S_2/S_1 order in polyenes.[12,13] Thus, experiment[14−17] and theory[7,8,12,13] agree that in linear polyenes the lowest excited state is the 2^1A_g state and that the energy gap between the 1^1B_u and 2^1A_g states increases with increasing chain length. This picture is slightly modified in the case of the all-*trans*-α,ω-diphenylpolyenes. The energy of the 1^1B_u state is lower than the energy of the 2^1A_g state in *trans*-stilbene, the two states are presumed nearly isoenergetic in all-*trans*-diphenylbutadiene (DPB), and the 2^1A_g state is the lowest excited state in all-*trans*-diphenylhexatriene (DPH) and the longer vinylogues.[3−5]

The lowest electronic transitions between the ground state and higher states of each type are the symmetry-allowed $1^1B_u \leftarrow 1^1A_g$ and the symmetry-forbidden $2^1A_g \leftarrow 1^1A_g$ transitions. Although forbidden by single-photon absorption, the $2^1A_g \leftarrow 1^1A_g$ transition is allowed through simultaneous two-photon excitation.[17] The forbidden $2^1A_g \rightarrow 1^1A_g$ emission from the excited 2^1A_g state is thought to occur via Herzberg−Teller vibronic coupling of the 2^1A_g and 1^1B_u states, which renders the transition partially allowed through reduction in symmetry and concurrent relaxation of the symmetry requirements.[18−20] For DPH in solution, an equilibrium mixture[21−23] of the 2^1A_g and 1^1B_u states is established within femtoseconds[24−26] following initial formation of the 1^1B_u state.

† On leave from Jagiellonian University, Faculty of Chemistry, 30 060 Cracow, Poland.

‡ Department of Chemistry and Biochemistry, University of Delaware, Newark, Delaware 19716.

10.1021/jp045201u CCC: $30.25 © 2005 American Chemical Society
Published on Web 12/23/2004

The experimental effective fluorescence rate constants, $k_f^{obs} = \phi_f^{obs}/\tau_f^{obs}$, of DPH and higher diphenylpolyenes, where the ϕ_f^{obs} values are measured fluorescence quantum yields and τ_f^{obs} values are measured fluorescence lifetimes, are much smaller than the corresponding theoretical radiative rate constants, $k_f^{th} = n^2 k_{f,0}^{th}$ (where $k_{f,0}^{th}$ is the $1^1B_u \rightarrow 2^1A_g$ fluorescence rate constant in the gas phase under isolated molecule conditions for which the index of refraction $n = 1$) based on the Strickler−Berg[27] or Birks−Dyson[28] relationships.[2−4] The Hudson−Kohler model nicely accounts for these discrepancies, because different electronic states are involved in the absorption and emission transitions. The observed fluorescence rate constant, k_f^{obs}, is primarily related to the forbidden $2^1A_g \rightarrow 1^1A_g$ transition, whereas the calculated rate constant, k_f^{th}, is for the allowed $1^1B_u \rightarrow 1^1A_g$ transition. The formally forbidden $2^1A_g \rightarrow 1^1A_g$ transition is considered to borrow probability from the allowed $1^1B_u \rightarrow 1^1A_g$ transition through vibronic mixing,[18,19] and to the extent that k_f^{obs} corresponds to the $2^1A_g \rightarrow 1^1A_g$ transition, it depends on the magnitude of the calculated rate constant, k_f^{th}, and on the degree of mixing between the 1^1B_u and 2^1A_g states and, thereby, on the $1^1B_u - 2^1A_g$ energy gap

$$k_f^{obs} = k_f^{th}\left(\frac{V_{ab}}{\Delta E_{ab}}\right)^2 \qquad (1)$$

where V_{ab} is the temperature- and solvent-independent[18,19] vibronic matrix coupling element between the 2^1A_g and 1^1B_u states, and ΔE_{ab} is the $1^1B_u - 2^1A_g$ energy gap. However, because observed DPH fluorescence quantum yields include contributions from the thermally populated 1^1B_u state[21−23] and from *s*-*c*-DPH,[29] k_f^{obs} values are expected to be larger than those given by eq 1 (strictly speaking, eq 1 gives $k_f^{S_1-S_0}$ for *s*-*t*-DPH). The presence of *s*-*c*-DPH fluorescence is evident in the λ_{exc} dependence of the fluorescence spectra,[29] a striking demonstration of Havinga's nonequilibration of excited rotamers (NEER) principle.[30]

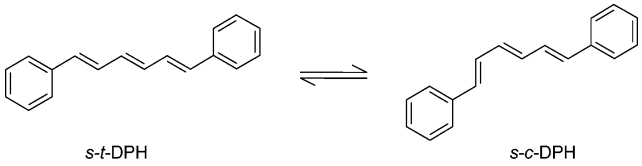

The aim of this paper is to achieve a quantitative evaluation of the fluorescence of DPH by resolving it into its three contributing emissions. Because two of these emissions originate from thermally populated states, their contribution in the spectrum can be varied by varying *T*. However, resolutions of spectrothermal matrices of DPH fluorescence spectra are thwarted because of *T*-dependent spectral broadening[31] and differential shifts[32] of the pure component spectra. *T*-induced differential shifts in DPH and higher diphenylpolyenes have their origin in the linear dependence of ΔE_{ab}, the $1^1B_u - 2^1A_g$ energy gap, on the polarizability, $\alpha = (n^2 - 1)/(n^2 + 2)$, of the solvent.[18,19,23,33−35] The 1^1B_u state, in which electron density is partially localized, is stabilized on increasing α (induced polarization[36]), while the highly correlated 2^1A_g state is insensitive to changes in α. Consequently, absorption and fluorescence excitation spectra shift to the red as solvent polarizability is increased (the $1^1B_u \leftarrow 1^1A_g$ transition), in contrast to the λ_{max} of the fluorescence spectra (in the main, the $2^1A_g \rightarrow 1^1A_g$ transition), which is insensitive to solvent changes.[33,37,38] As expected, the intensity and position of the thermally activated 1^1B_u fluorescence, observed in DPH and its derivatives as a weak band at the leading edge of the fluorescence spectrum, shifts to the red and becomes more pronounced with increasing medium polarizability.[21−23,39]

In this paper, we accomplish the PCA-SM resolution of DPH fluorescence by (a) avoiding spectral shifts by measuring the DPH fluorescence spectra in *n*-alkanes (C_n, using C_8 to C_{16} with *n* even) at *T* values selected to keep the index of refraction constant (hence, varying *s*-*c*-DPH/*s*-*t*-DPH and $1^1B_u/2^1A_g$ ratios under isopolarizability conditions), (b) independently varying the *s*-*c*-DPH/*s*-*t*-DPH ratio by changing λ_{exc}, (c) compensating for thermal broadening, and (d) applying van't Hoff linearity SM constraints. We also report fluorescence quantum yields and lifetimes under isopolarizability conditions.

Experimental Section

Materials. all-*trans*-1,6-Diphenyl-1,3,5-hexatriene from Aldrich, 98% purity, was chromatographed on silica gel with ethyl acetate/petroleum ether (1:99 v/v) as eluent and then twice recrystallized from *n*-hexane (Aldrich, spectrophotometric grade). Petroleum ether from Baker, reagent grade, was distilled prior to usage. *n*-Alkanes (*n*-octane, *n*-decane, *n*-dodecane, *n*-tetradecane, and *n*-hexadecane) from Aldrich (anhydrous, 99+%) were used as received.

Measurements. Fluorescence measurements for the spectral resolution were made with a modified[40] Hitachi/Perkin-Elmer MPF-2A spectrophotometer equipped with a 150-W Xe arc source and a Hamamatsu R106UH photomultiplier tube and for quantum yield measurements with a Hitachi F-4500 spectrophotometer equipped with a 150-W Xe arc source and a Hamamatsu R3788 photomultiplier tube (the Hitachi F-4500 employs horizontal excitation and emission slits instead of vertical). UV−vis absorption spectra were measured with a Perkin-Elmer Lambda-5 or a Cary 300 spectrophotometer. All spectrophotometers were interfaced to Dell microcomputers.

Aliquots (4-mL) of DPH in *n*-alkane solvents (with [DPH] $\approx 0.58 \times 10^{-5}$ M) were pipetted into 13-mm o.d. Pyrex ampules equipped with standard 1-cm^2 quartz fluorescence cell sidearms. The samples were degassed (4 freeze−pump−thaw cycles) and flame-sealed at a constriction. Sample preparation and handling were performed under nearly complete darkness (red light). Fluorescence spectra for the spectrothermal matrix were recorded at ~2-nm increments in the λ_{exc} ranges of 300.3−317.7 and 381.5−398.9 nm producing 10 spectra in each range. Fluorescence intensities were collected in the 350−600-nm range in 0.25-nm increments. Fluorescence quantum yields were determined using quinine sulfate in 1 N H_2SO_4 ($\phi_f = 0.546$ at 25 °C)[41,42] as the reference standard. Fluorescence spectra of DPH for the spectrothermal matrix were measured at 284.0 K in *n*-octane, 316.6 K in *n*-decane, 340.2 K in *n*-dodecane, 359.4 K in *n*-tetradecane, and 372.5 K in *n*-hexadecane. The indexes of refraction measured at these temperatures were approximately constant and equal to 1.4020 ± 0.0001. Temperatures were maintained to within ± 0.1 °C using a Haake-FN constant *T* circulator or a Neslab-RTE 4DD circulation bath. Solution temperatures were measured with an Omega Engineering model 199 RTD digital thermometer.

Fluorescence lifetimes were measured with degassed samples, as previously described,[43] with a phase modulation Fluorolog-τ2 lifetime spectrofluorometer (SPEX) equipped with a 450-W Xe arc source, a Hamamatsu R928P photomultiplier tube, and a Lasermetrics BNC 1072FW Pockel cell (KD_2PO_4).

Data Analysis. Data pretreatment and PCA-SM calculations were performed on a Dell microcomputer working with ap-

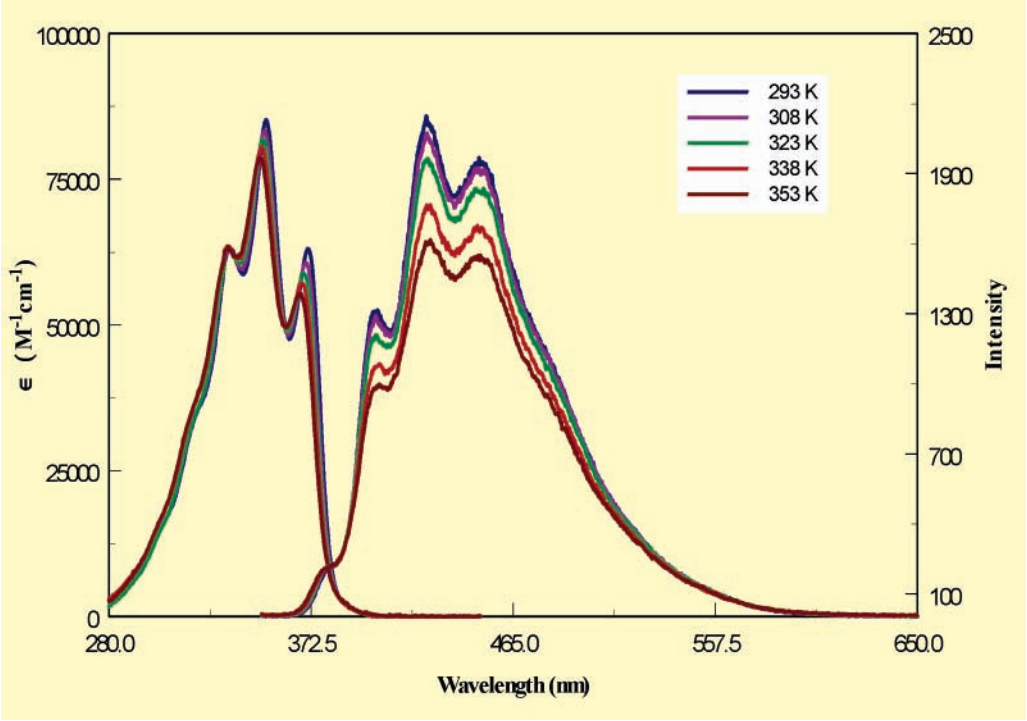

Figure 1. Fluorescence and absorption spectra of DPH in *n*-octane as a function of *T*.

propriate routines in the environment of *MATLAB* packages, versions 5.2 and 6.1.

Computational Details. Calculations were carried out using *Gaussian 98*[44] utilizing gradient geometry optimization.[45] All geometries were fully optimized using the B3LYP functional[46,47] with the 6-311+G(d,p) basis set. Frequencies, zero-point vibrational energy corrections (ZPVE), and enthalpies were calculated at the same level of theory.

Results

Fluorescence and absorption spectra in C_8 as a function of *T* and fluorescence spectra in the C_n series under isopolarizability conditions are shown in Figures 1 and 2, respectively. The fluorescence spectra were baseline corrected by subtracting the emission of corresponding solvent blanks following removal of interfering prominent Rayleigh and Raman scattered light peaks. Scattered light correction was performed by PCA treatment of partial spectral matrices composed of DPH or solvent blank spectra having no spikes in the λ region of DPH fluorescence. The resulting most significant eigenvectors were then used to reconstruct the scattered-light-affected λ portions of subsequent spectra by least-squares fitting.[40] Each corrected spectrum was in turn used to augment the initial partial matrix, while an old spectrum was removed, keeping the matrix size unchanged. The DPH fluorescence spectra were then corrected for self-absorption in the short λ region by use of absorption spectra measured under the same conditions.

The s-c-DPH Conformer Fluorescence Spectrum. As previously observed for DPH in methylcyclohexane (MCH), excitation at the onset of DPH absorption, $\lambda_{exc} \geq 380$ nm, leads to a significant increase in the contribution of s-cis conformer emission in DPH fluorescence spectra.[40] Pure *s-c*-DPH fluorescence spectra in C_n under isopolarizability conditions were obtained by following a similar procedure to that described earlier.[40] The background and baseline-corrected DPH fluorescence spectra were normalized to unit area, and the spectra recorded for low and high excitation ranges were averaged

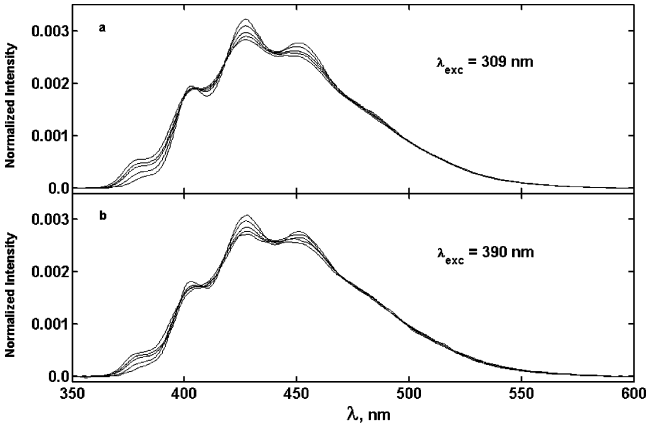

Figure 2. Fluorescence spectra of DPH in five *n*-alkane solvents at five different temperatures (see text) for excitation lines in the range 300.3−317.7 nm (A) and in the range 381.5−398.9 nm (B).

separately, producing for each range one characteristic averaged spectrum, nominally assigned to the average excitation wavelengths of 309.0 and 390.2 nm, respectively. A pair of normalized spectra was thus obtained at its characteristic isopolarizability temperature, Figure 2, for each *n*-alkane solvent. Comparison of the low (309 nm) and high (390 nm) λ_{exc} range fluorescence spectrum for each solvent reveals that the 390-nm spectrum is less intense at the short λ onset and more intense at the long λ tail than the corresponding 309-nm spectrum.

The spectra in Figure 2 were compensated for *T*-dependent broadening by applying the method that was used recently in the resolutions of spectrothermal matrices composed of 1,3-butadiene vapor-phase UV absorption spectra[31] and benzophenone luminescence spectra.[48] The broadening compensation procedure is only briefly described here, because it has been presented in detail elsewhere.[31] It involves the derivation of a set of thermal spread functions (normalized *T* characteristic Gaussian functions), which on convolution with the corresponding spectra leads to a nearly uniformly broadened set of spectra, each having the broadening expected at the highest experimental

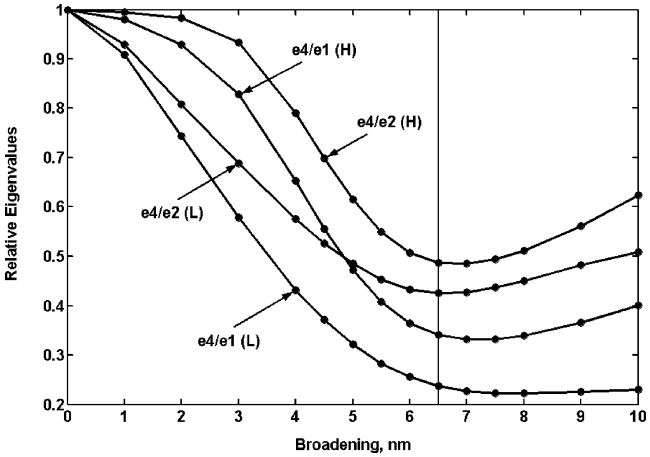

Figure 3. Evolution of eigenvalue ratios with the extent of broadening compensation applied to the DPH spectrothermal data matrix (Figure 2a,b).

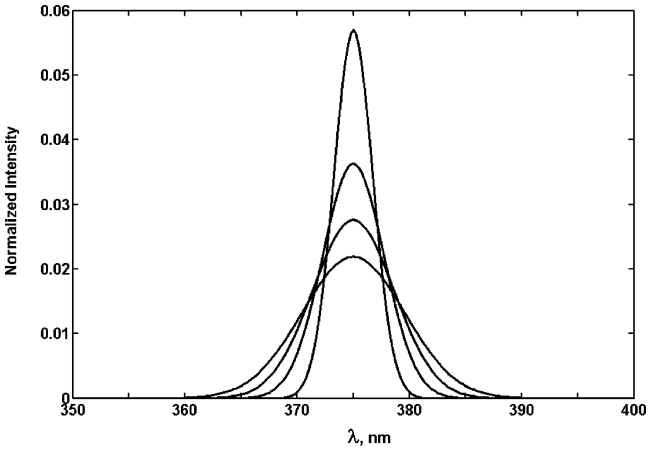

Figure 4. The optimum set of spread functions.

temperature. Because the spread functions are derived from a single basic spread function on the basis of the *T* dependence of broadening, the search for the optimum set requires identification of only one parameter (*k* in eq 9 of ref 31). PCA treatment of the sets of broadening compensated spectra formed for each selected value of the broadening parameter *k* are evaluated by tracing the evolution of the ratios of the most significant eigenvalues. Specifically, when a three-component system is ideally expected, as in the DPH case, the objective of broadening compensation is to minimize the importance of the fourth and higher components that reflect nonlinear spectral changes. This is achieved by selecting the broadening parameter that minimizes the relative magnitude of the fourth eigenvalue (ev4). Indeed, as shown in Figure 3, plots of ev4/ev2 versus *k* define nearly identical minima at $k = 6.5$ cm^{-1} (full width at half-maximum of the reference thermal spread function) for both sets of spectra in Figure 2. The selected optimum set of spread functions is shown in Figure 4, and the effect of broadening compensation with the use of this set on the eigenvectors shown in Figure 5. The success of the procedure is reflected in the pronounced suppression of oscillatory features in the second and third eigenvectors, a second essential criterion revealed by analogous treatments of simulated spectral matrices.[31] No such smoothing is observed in the fourth and subsequent eigenvectors, which are neglected in the analysis.

The *s*-*c*-DPH fluorescence spectrum for each solvent was obtained as previously described[29] by subtraction of the low (309 nm) from the corresponding high (390 nm) λ_{exc} compensated fluorescence spectrum following normalization of each pair in the 360−375 nm region (equal areas in that region). This yielded excellent baselines, indistinguishable from zero, in the selected spectral region and nearly solvent-independent difference spectra for *s*-*c*-DPH fluorescence. The result for *n*-dodecane, illustrated in Figure 6, is typical.

The A_g/B_u Spectral Mixtures. The *s*-*t*-DPH fluorescence spectrum (a $2A_g/1B_u$ spectral mixture) was obtained in each *n*-alkane solvent by PCA-SM treatment of the corresponding normalized (unit area) set of three spectra, shown for C_{12} in Figure 6: the low- and high-λ_{exc} spectra and the *s*-*c*-DPH spectrum. SM was carried out by moving on the α,β normalization line toward the expected location of the combination coefficients of the *s*-*t*-DPH spectrum (a solvent/*T*-specific $2A_g/1B_u$ spectral mixture). Selection of the pure $2A_g/1B_u$ mixture spectrum from 200 or more candidates in each solvent was based on the requirement that the predicted ratios of *s*-*cis*- and *s*-*trans*-DPH contributions ($x_{s-c,i}/x_{s-t,i}$, where *i* designates λ_{exc}) for the low- and high-λ_{exc} spectra simultaneously correspond to the two best fit van't Hoff plots describing the equilibrium between these conformers.[31,48−50] As a secondary criterion, care was taken to ensure that the choice was among spectra that did not violate the Lawton and Sylvestre nonnegativity criterion.[51] The van't Hoff equation used in the optimization process is given by

$$R \ln\left(\frac{x_{s-c,i}}{x_{s-t,i}}\right) = R \ln\left(\frac{\epsilon_{s-c,i}\phi_{s-c}}{\epsilon_{s-t,i}\phi_{s-t}}\right) + \Delta S - \frac{\Delta H}{T} \qquad (2)$$

where $\epsilon_{s-c,i}$ and $\epsilon_{s-t,i}$ are the decadic molar absorptivities of the s-trans and s-cis conformers, respectively, $\phi_{s-c,i}$ and $\phi_{s-t,i}$ are the corresponding fluorescence quantum yields of the two conformers at the effective isopolarizability *T* in each solvent, *R* is the ideal gas constant, and ΔS and ΔH are the entropy and enthalpy differences between the two conformers. The best fit gives $\Delta H = 2.83$ kcal/mol for both plots with satisfactory correlation coefficients equal to 0.998 (lower plot for $\lambda_{exc} = 390$ nm) and 0.994 (upper plot for $\lambda_{exc} = 390$ nm), Figure 7. The resulting optimum set of *s*-*t*-DPH spectra, consisting of different mixtures of 2^1A_g and 1^1B_u fluorescence, is shown in Figure 8. The increase in 1^1B_u fluorescence contribution with increasing isopolarizability *T* can readily be seen at the onset of the spectra in Figure 8.

Pure 2^1A_g and 1^1B_u Fluorescence Spectra. Assuming a Boltzmann distribution for the population of the two lowest excited singlet states of *s*-*t*-DPH,[23,52] the ratio of $1^1B_u \rightarrow 1^1A_g$ to $2^1A_g \rightarrow 1^1A_g$ fluorescence intensities, F_b and F_a, respectively, should obey eq 3

$$R \ln\left(\frac{x_b}{x_a}\right) = R \ln\left(\frac{k_{fb}}{k_{fa}}\right) - \frac{\Delta E_{ab}}{T} \qquad (3)$$

where x_b and x_a, the fractional contribution of 1^1B_u and 2^1A_g fluorescence, respectively, are used instead of the spectral areas F_b and F_a, and k_{fa} and k_{fb} are the corresponding radiative rate constants. The fluorescence spectra in Figure 8 were resolved into pure 2^1A_g and 1^1B_u spectra by PCA-SM by imposing optimum fit to eq 3 as the SM constraint. The procedure is analogous to the application of the van't Hoff plot optimization SM constraint described already. The best fit plot to eq 3 is shown in Figure 9. The slope of the line in Figure 9 gives $\Delta E_{ab} = 4.13$ kcal/mol, which corresponds to 1446 cm^{-1}, and the intercept is 8.23 cal/(mol K). The linearity of the plot in Figure 9 is exact (correlation coefficient with nine nines!) because it is based on fractional contributions found by moving along the

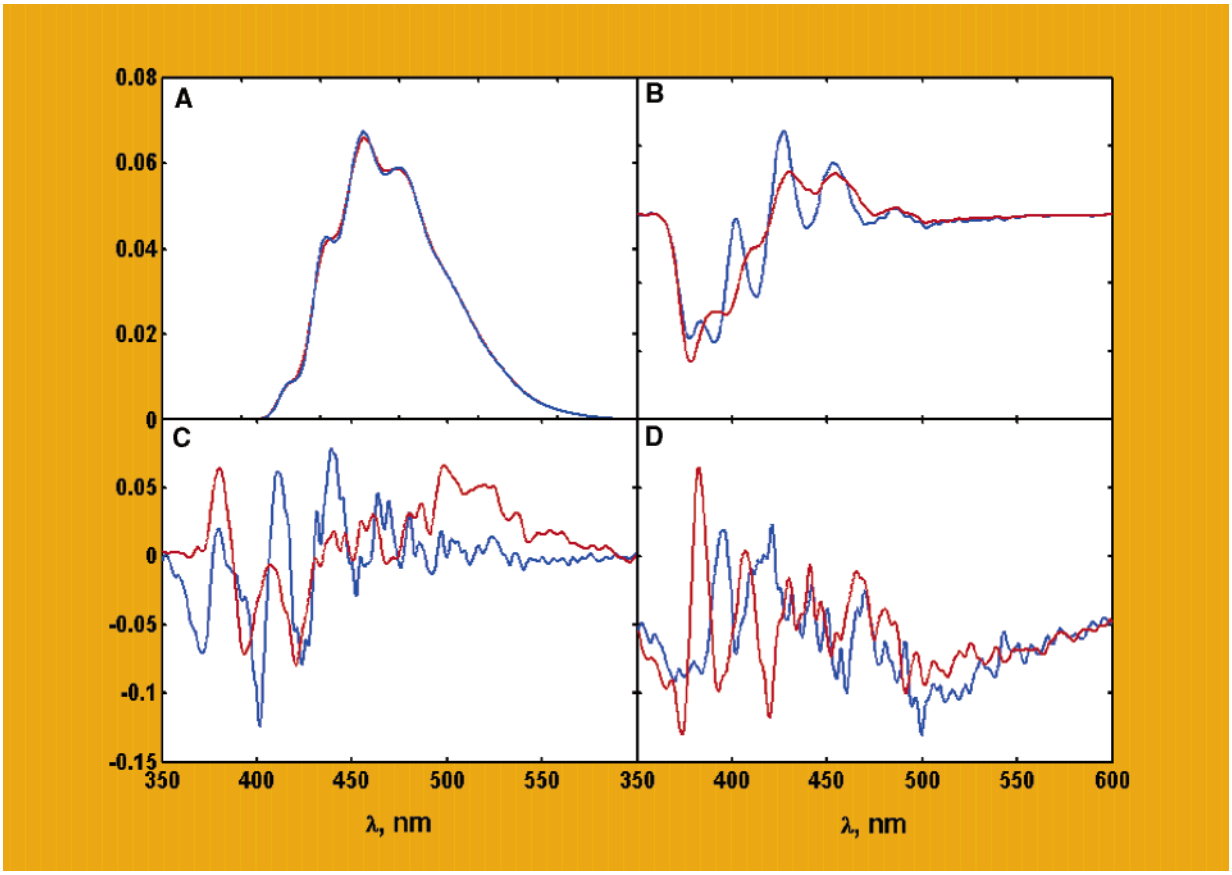

Figure 5. Pairwise comparison of the first four eigenspectra (in ascending order from A to D) obtained for the DPH spectrothermal data matrix before (blue lines) and after (red lines) optimum compensation for broadening.

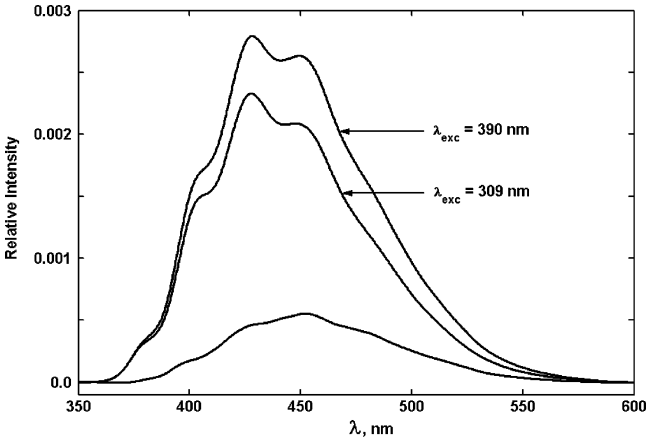

Figure 6. Difference spectrum (*s*-*c*-DPH) obtained in *n*-dodecane by normalizing high and low excitation wavelength fluorescence spectra at the onset region (350−375 nm).

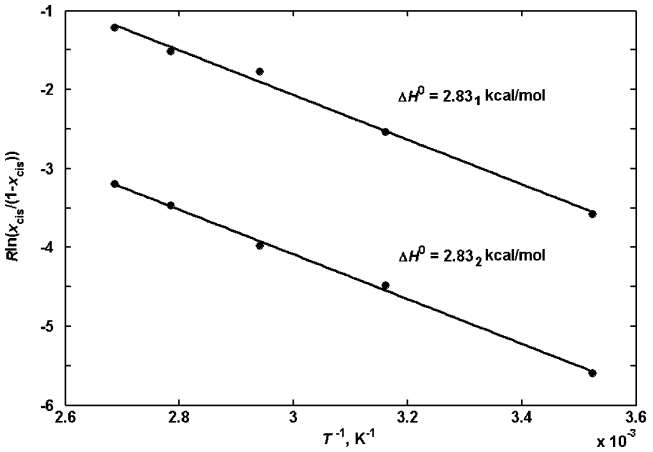

Figure 7. Simultaneously optimized van't Hoff plots for the equilibration between s-trans and s-cis conformers of DPH for low (lower fit) and high (upper fit) excitation wavelengths.

α,*β* normalization line for the spectra in Figure 8. A more realistic plot, based on the x_b/x_a ratios for the actual spectra (Table 1) gives $\Delta E_{ab} = 4.09 \pm 0.11$ kcal/mol and an intercept of 7.87 ± 0.34 cal/(mol K). The significance of the intercept will be considered in the Discussion section.

The resolved spectra (corrected for nonlinearity in instrumental response), that is, the 2^1A_g and 1^1B_u pure component fluorescence spectra from the all-s-trans conformer, and the s-cis,s-trans conformer fluorescence spectrum (taken as the average of the *s*-*c*-DPH fluorescence spectra in the five *n*-alkanes) are shown in Figure 10. Also shown in Figure 10 is the absorption spectrum of DPH in *n*-octane (mostly the $1^1B_u \leftarrow 1^1A_g$ transition). These resolved spectra correspond to the highest experimental $T = 372.4$ K used in this study. PCA treatment of the fluorescence spectra in Figures 2, 6, and 8 reveals a three-component system, as expected. Combination coefficients of the spectra in α,*β*,*γ* eigenvector space are shown in Figure 11. The combination coefficients of the three pure-component spectra define the corners of the triangle in the normalization plane (labeled 2^1A_g, 1^1B_u, and *s*-*c*-DPH in Figure 11). Points on the $2^1A_g/1^1B_u$ line correspond to the spectral mixtures in Figure 8, and points inside the triangle, lying along solvent/*T* specific lines starting at the corner for the *s*-*c*-DPH fluorescence spectrum and intersecting the $2^1A_g/1^1B_u$ side, represent the experimental spectra in Figure 2. Fractional contributions of the three components in the individual spectra,

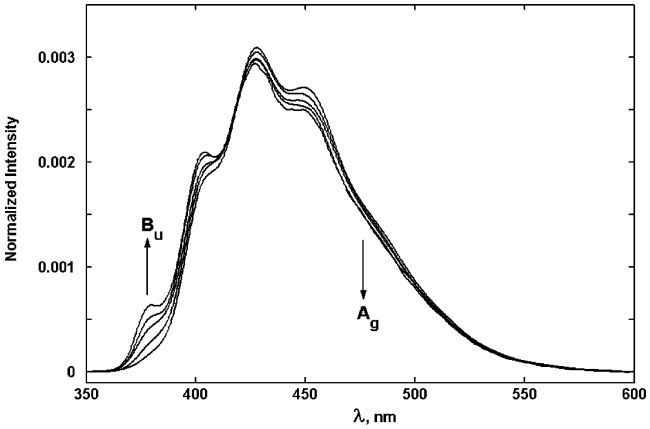

Figure 8. Resolved *s*-*t*-DPH fluorescence spectra (A_g/B_u mixtures) in C_n at isopolarizability *T*s (see text).

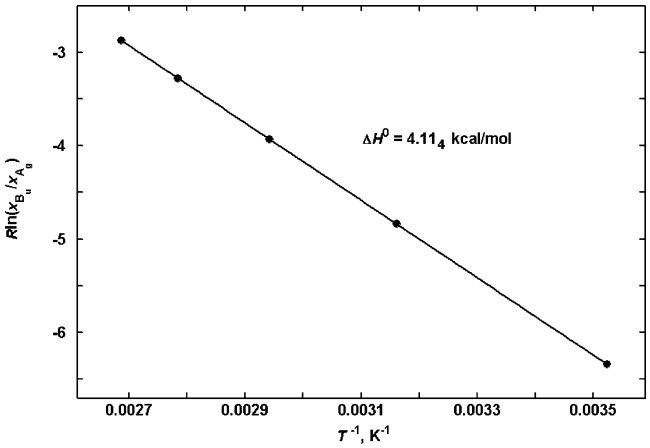

Figure 9. Optimum van't Hoff (Boltzmann) plot for thermal equilibration between the A_g and B_u excited singlet states of *s*-*t*-DPH.

TABLE 1: Pure Component Fractional Contributions in the DPH Spectra in Figures 2 and 8[a]

excitation or composition	*T* [K]	x_A	x_B	x_C	$\sum x_i$
$\lambda_{exc} = 309$ nm	284.0	0.8795	0.0361	0.0844	1.0000
	316.6	0.8552	0.0616	0.0832	1.0000
	340.2	0.7839	0.0950	0.1211	1.0000
	359.4	0.7295	0.1129	0.1577	1.0001
	372.5	0.6983	0.1427	0.1590	1.0000
$\lambda_{exc} = 390$ nm	284.0	0.7637	0.0367	0.1996	1.0000
	316.6	0.7249	0.0525	0.2226	1.0000
	340.2	0.6451	0.0741	0.2809	1.0001
	359.4	0.5801	0.0785	0.3414	1.0000
	372.5	0.5698	0.1101	0.3201	1.0000
A_g/B_u mixtures	284.0	0.9536	0.0361	0.0103	1.0000
	316.6	0.9479	0.0705	0.0184	1.0368
	340.2	0.8775	0.1106	0.0119	1.0000
	359.4	0.8652	0.1447	0.0099	1.0198
	372.5	0.8187	0.1730	0.0084	1.0001

[a] Spectral contributions are based on spectra that are corrected for nonlinearity in instrumental response.

corrected for nonlinearity of instrumental response, are given in Table 1. The fit of the broadened 390-nm spectrum of DPH in C_{16} in terms of the pure component contributions is typical, Figure 12.

In Figure 10, the absorption spectrum of DPH in *n*-octane was scaled to match the height of its first band to the height of the first band of the 1^1B_u fluorescence spectrum. The matched spectra reveal excellent Levshin mirror symmetry[53] in their vibronic patterns. The position of the first band in the 1^1B_u

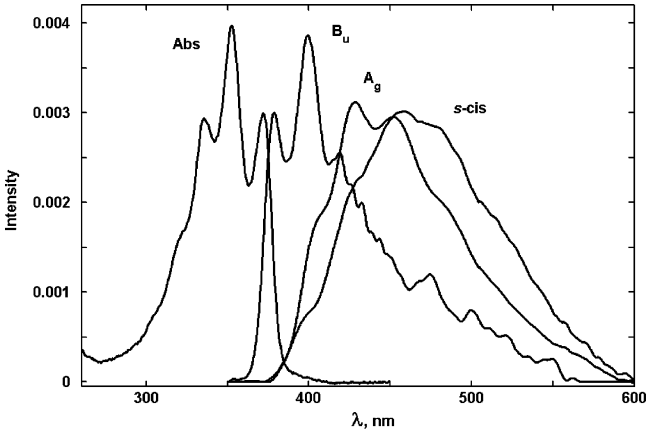

Figure 10. Pure-component DPH fluorescence spectra (corrected for nonlinearity of instrumental response) and the absorption spectrum of DPH in *n*-octane.

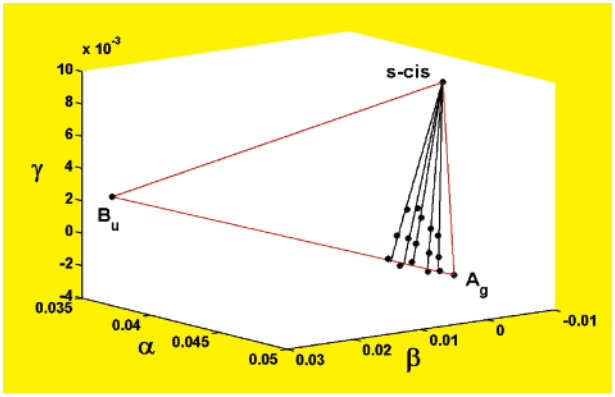

Figure 11. Normalization plane with pure components defining the corners of the triangle: A_g, emission from the s-trans 2^1Ag state; B_u, emission from the s-trans 1^1B_u state; and s-cis conformer emission. The point on the $2^1A_g/1^1Bu$ mixture line closest to the A_g corner corresponds to *n*-octane.

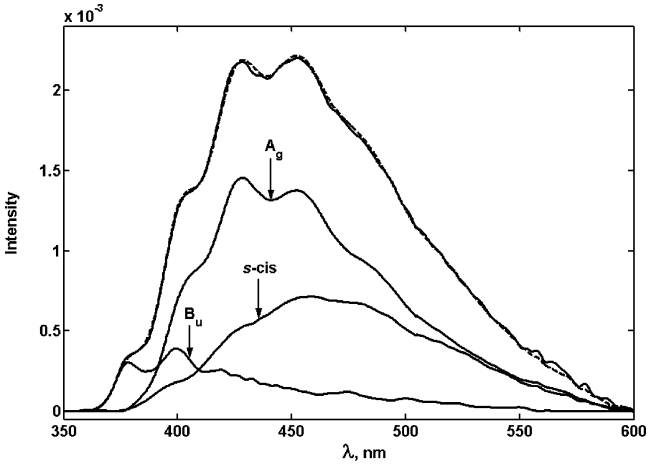

Figure 12. The 390-nm fluorescence spectrum of DPH (solid line) in C_{16} at 359.2 K and reproduced (dashed line) as the sum of the pure component contributions.

emission spectrum is 378.5 nm, and that of the first band of the 2^1A_g emission spectrum, determined by fitting five Gaussian envelopes to the spectrum of the $1^1A_g \leftarrow 2^1A_g$ emission, is 403.1 nm. The energy difference between these two bands is 1615 cm^{-1}.

Fluorescence Quantum Yields and Lifetimes. Fluorescence quantum yields ([DPH] = 2×10^{-6} M) and lifetimes ([DPH] = 2×10^{-5} M) in degassed *n*-alkanes are given in Table 2.

TABLE 2: Fluorescence Quantum Yields and Lifetimes for DPH in C_n under Isopolarizability Conditions[a]

C_n	T, K	ϕ_f	τ_f,[b] ns	k_f^{obs}, 10^7 s^{-1}	k_f,[d] 10^7 s^{-1}
C_8	284.0	0.71	15.7	4.5	4.5 (4.5)
C_{10}	316.6	0.70	14.1	4.9	4.7 (4.5)
C_{12}	340.2	0.68	13.6	5.0	4.9 (4.6)
C_{14}	359.4	0.70	12.7	5.5	5.0 (4.7)
C_{16}[c]	372.5	(0.73)	12.3	(5.9)	5.2 (4.7)

[a] Excitation wavelengths were 365 and 355 nm for quantum yields and lifetimes, respectively; for lifetimes, $\lambda_{em} = 450$ nm. [b] Values of χ^2 were in the 1.03−1.20 range. [c] The ϕ_f value is extrapolated from measurement in the 293−343 K range, and the τ_f value is for 293 K. [d] Calculated from eq 5, see text; values in parentheses for $k_f^{th} = 9 \times 10^8$ s^{-1}.

TABLE 3: Fluorescence Quantum Yields and Lifetimes for DPH in *n*-Dodecane

T, K	λ_{exc}, nm	λ_{em}, nm	τ_f,[b] ns	χ^2	ϕ_f[a]
293.2	355	450	13.6	1.09	0.73 (0.71)
313.2	380	525	13.9	1.03	0.72 (0.72)[b]
323.2	355	450	13.6	1.16	0.71 (0.67)
343.2	355	450	13.5	1.06	0.68 (0.66)[c]
343.2	380	525	13.5	1.12	0.65 (0.66)[d]

[a] $\lambda_{exc} = 365$ nm; values in parentheses are for $\lambda_{exc} = 380$ nm. [b] $T = 308.2$ K. [c] $T = 338.2$ K. [d] $T = 353.2$ K.

They were measured at the isopolarizability Ts, except for C_{16}, for which the quantum yield was extrapolated from measurements at lower Ts and the lifetime was measured at 293 K. Lifetimes were shown to be independent of T and of excitation ($\lambda_{exc} = 355$ and 380 nm) and monitoring λ ($\lambda_{em} = 450$ or 525 nm) in C_{10} and C_{12} (293−343 K). The results in Table 3 for C_{12} are typical. Within ±5% experimental uncertainty, the fluorescence quantum yields are also independent of λ_{exc} (365 or 380 nm).

Discussion

In addition to its use as a polyene model,[54] DPH has been used widely in photophysical studies as a probe of the microenvironment.[55] The results presented in this paper provide for the first time the quantitative resolution of DPH fluorescence spectra into its three components: the $2^1A_g \rightarrow 1^1A_g$ and $1^1B_u \rightarrow 1^1A_g$ fluorescence spectra of *s*-*t*-DPH and the emission of *s*-*c*-DPH, Figure 10. We succeeded in this task by applying PCA-SM to a spectrothermal matrix, composed of spectra measured under isopolarizability conditions to eliminate differential spectral shifts and uniformly broadened by compensation for T-induced thermal broadening. To appreciate the impact of differential shifts on the emission spectra, one need only compare the onsets of Figures 1 and 2. Although similar T ranges are involved, the 1^1B_u fluorescence intensities at the short λ onset are remarkably T-independent in *n*-octane (Figure 1), whereas they increase strongly with increasing T in the *n*-alkane series (Figure 2). Paradoxically, although the $1^1B_u \rightarrow 1^1A_g$ is thermally activated, its absolute contribution to the fluorescence spectrum is T-independent in a single *n*-alkane solvent. The coincidence here is that the expected increase in the Boltzmann population of the 1^1B_u state with increasing T is nearly exactly canceled by (1) the increase in ΔE_{ab}, caused by the accompanying drop in polarizability and (2) the decrease in the overall population of excited *s*-*t*-DPH due to the drop in its ground-state equilibrium concentration. The change in ΔE_{ab} is almost entirely due to the relative destabilization of the 1^1B_u state with decreasing α, as seen in Figure 1 in the shifts of the $1^1B_u - 1^1A_g$ transitions in absorption and emission. On the other hand, with ΔE_{ab} constant under isopolarizability conditions, the expected increase in the contribution of the $1^1B_u \rightarrow 1^1A_g$ transition with increasing T is readily seen in Figure 2. We stress here that because of the T-induced differential nonlinear changes in the pure-component fluorescence spectra, Figure 1 exemplifies a type of spectrothermal matrix that cannot be resolved by PCA-SM treatment. Attempts by others[56] to resolve such matrices by PCA-SM have failed.[57]

The implications of our results are considered in the following text.

Havinga's NEER Principle. The discovery that, contrary to earlier reports,[37,38,58] the fluorescence spectrum of DPH is λ_{exc}-dependent allowed resolution of *s*-*c*-DPH and *s*-*t*-DPH fluorescence spectra in MCH.[29] Ground-state conformer control of excited-state behavior was postulated first by Havinga to account for the λ_{exc} dependence of photoproduct distributions in conjugated trienes in the vitamin D field.[30] The resolution of the DPH conformer fluorescence spectra provided the first direct confirmation of Havinga's NEER principle as applied to the singlet excited states of a triene system. Results in the 3.9−91.0 °C range with λ_{exc} of 355 and 385 nm gave $\Delta H = 2.95 \pm 0.11$ and 3.29 ± 0.17 kcal/mol, respectively, as the conformer enthalpy difference.[29] Our observations in the *n*-alkane series under isopolarizability conditions confirm the λ_{exc} effect, Figure 2, and give $\Delta H = 2.83$ kcal/mol, Figure 6, in good agreement with the values for MCH and with the value of 2.93 kcal/mol for *s*-*trans*/*s*-*cis*-1,3-butadiene equilibration in the gas phase.[31] DFT calculations (B3LYP/6-311+G(d,p)) reveal structures and energies for stationary-state geometries in S_0 of DPH in reasonable agreement with the experimental results, Figure 13. The global minimum is located at the planar *s*-*t*-DPH geometry, whose calculated structure is in excellent agreement with the X-ray crystallographic structure of DPH.[59] A transition state (TS) at the planar *s*-*c*-DPH geometry connects two slightly nonplanar, energetically equivalent, enantiomeric conformers (+)*s*-*c*-DPH (<CCCC = 14.6; <CCCC = 6.9) and (−)*s*-*c*-DPH (<CCCC = −14.6; <CCCC = −6.9). The extremely low barrier for enantiomeric interconversion through the planar *s*-*c*-DPH indicates that the potential energy surface is very flat in that region and that *s*-*c*-DPH can readily adopt both entirely planar and slightly nonplanar geometries. It is worth noting that the imaginary frequency, 14.9i cm^{-1}, at the planar geometry is so negligibly small that the planar *s*-*c*-DPH structure may be considered a minimum. This is consistent with the fact that the enthalpy of the planar structure is ~0.5 kcal/mol lower than that of the nonplanar *s*-*c*-DPH structures. At 298.15 K, the enthalpy difference between *s*-*c*-DPH and *s*-*t*-DPH conformers is predicted to be 3.4 kcal/mol (see Table 1S in Supporting Information). Initial calculations with the 6-31G(d) basis set yielded a value of 3.15 kcal/mol.

Adherence to the NEER postulate shows that despite relatively long lifetimes (12−16 ns, Table 2), both the 1^1B_u and the 2^1A_g singlet excited states maintain structural integrity with respect to rotation about ground-state essential single bonds. It stands to reason that the much shorter lived lowest singlet excited states of the parent hexatriene[54] and alkylhexatrienes will similarly prevent ground-state rotamer equilibration.

The $1^1A_g \leftarrow 1^1B_u$ Fluorescence Spectrum. The very good mirror image symmetry between the recovered $1^1A_g \leftarrow 1^1B_u$ fluorescence spectrum and the absorption spectrum of DPH in *n*-octane (selected because it was recorded at the lowest T and is least contaminated by *s*-*c*-DPH absorption) validates our broadening compensation procedure. It confirms the assumption of mirror symmetry that was used by Itoh and Kohler[23] to

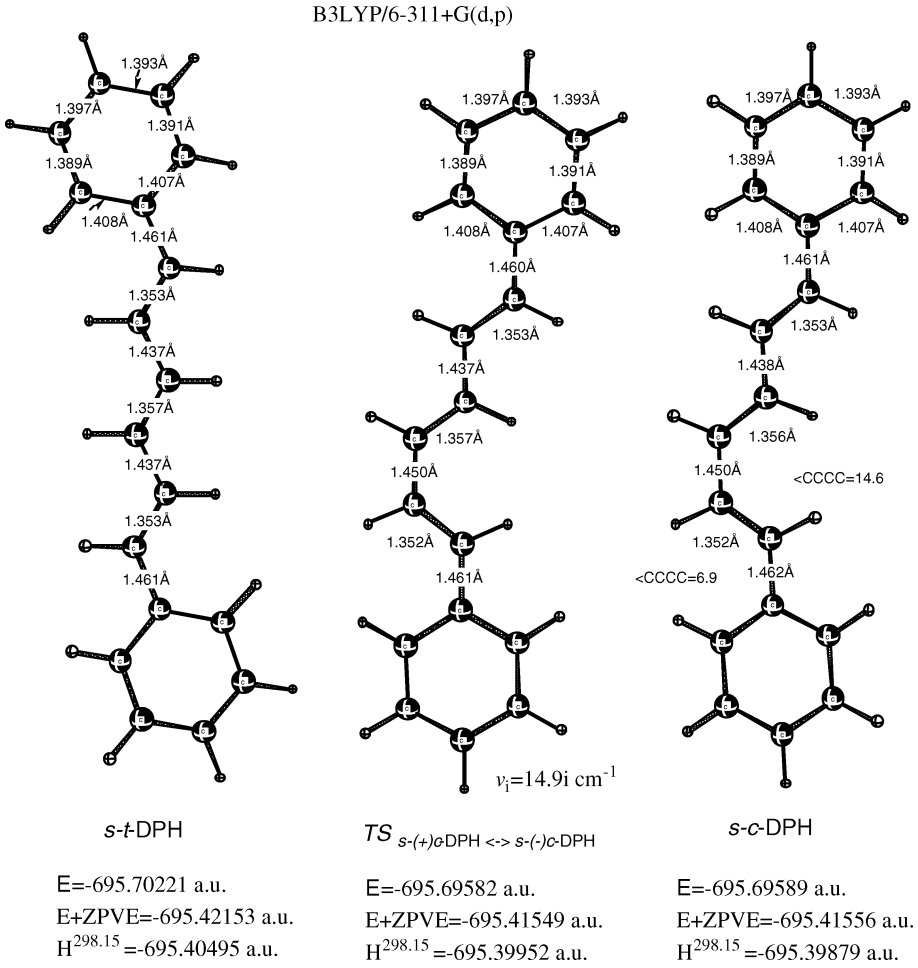

Figure 13. Stationary point geometries on the DPH S_0 surface, including the planar *s-c*-DPH "transition state" structure for interconversion between two gauche nonplanar (±)*s-c*-DPH enantiomers (see text; *s-t*-DPH is planar).

evaluate the *T*-dependence of the intensity ratio of 1^1B_u to 2^1A_g fluorescence from DPH spectra in *n*-hexane. However, that analysis neglected the overlapping contributions of *s-c*-DPH fluorescence. Without applying broadening compensation, our attempts to resolve the spectra in Figure 2 by PCA-SM treatment failed miserably. The impact of imposing nearly uniform broadening on the spectra is evident in the significantly dampened oscillations of the second and third principal eigenvectors, Figure 5.

The $2^1A_g \rightarrow 1^1A_g$ Fluorescence Spectrum. Except for the relative intensity of vibronic bands, the resolved $2^1A_g \rightarrow 1^1A_g$ fluorescence spectrum bears an uncanny resemblance to the resolved *s-c*-DPH fluorescence spectrum, Figure 10. The positions of the vibronic bands are nearly identical, and both spectra are characterized by relatively weak shoulders at the short wavelength onsets (weaker in *s-c*-DPH). The Franck−Condon envelopes of both spectra bear a strong similarity to the fluorescence spectrum of DPH seeded in helium in a supersonic band that was assigned by Kohler and Spiglanin to the $2^1A_g \rightarrow 1^1A_g$ transition in the isolated molecule.[15] Except for a roughly 300-cm^{-1} blue shift and slightly better vibronic definition, the relative intensities of the vibronic bands of the gas-phase spectrum suggest that it includes a substantial *s-c*-DPH fluorescence contribution. In view of the fact that the expansion involved DPH vapor at 445 K, this is not surprising.

The Matrix Coupling Parameter V_{ab}. There have been several attempts to determine V_{ab}, the vibronic matrix coupling element between the 2^1A_g and 1^1B_u states. With one exception, they have been based on eq 1 and the predicted polarizability dependence of experimental radiative rate constants, $k_f^{obs} = \phi_f^{obs}/\tau_f^{obs}$,[38] and have yielded rather high V_{ab} values. Chronologically, values of 245, 555, 745, 480, and 840 cm^{-1} were obtained in this way by Hudson and Kohler,[60] Andrews and Hudson,[18] Birks et al.,[19] Alford and Palmer,[61] and Bondarev and Bachilo,[62] respectively. These derivations employ estimated ΔE_{ab} values from the absorption and fluorescence spectra and neglect the thermally populated 1^1B_u and *s-c*-DPH fluorescence contributions by assigning the effective k_f^{obs} entirely to the $2^1A_g \rightarrow 1^1A_g$ transition. The method used to estimate ΔE_{ab} values alone can lead to large discrepancies. For instance, the 840-cm^{-1} value was based on overestimated ΔE_{ab} values taken from the apparent Stokes shift between first band maxima in the absorption ($1^1B_u \leftarrow 1^1A_g$) and fluorescence spectra (mainly $2^1A_g \rightarrow 1^1A_g$).[62] On the other hand, the intermediate 480-cm^{-1} value was based on significantly lower ΔE_{ab} values, because relaxation of the initial Franck−Condon (FC) states was considered. The difficulty of assigning ΔE_{ab} values on the basis of the spectra alone is evident in our results. The energy difference in the positions of the first bands in the resolved $1^1B_u \rightarrow 1^1A_g$ and $2^1A_g \rightarrow 1^1A_g$ fluorescence spectra, 1615 cm^{-1} (Figure 10) is significantly higher than 1431 cm^{-1}, the value obtained directly from the *T* dependence of $1^1B_u/2^1A_g$ fluorescence area ratios under isopolarizability conditions, Figure 9. This discrepancy is probably due to the fact that spectral determination of ΔE_{ab} requires having the absorption and the fluorescence spectra for the two transitions, because it is from their overlap that the positions of the 0−0 bands can be

estimated. The FC envelopes of the pure $1^1B_u \rightarrow 1^1A_g$ and $2^1A_g \rightarrow 1^1A_g$ fluorescence spectra, Figure 10, are very different. The $1^1B_u \rightarrow 1^1A_g$ spectrum has a relatively strong well-resolved 0−0 band and, relative to the corresponding absorption, reveals a rather small Stokes shift. In contrast, the initial band in the $2^1A_g \rightarrow 1^1A_g$ fluorescence spectrum appears as a weak shoulder, and the spectrum is generally less structured, leading to the expectation of a much larger Stokes shift. The difference in vibronic patterns also suggests smaller equilibrium geometry differences between the planar[59] 1^1A_g ground state, Figure 13, and the 1^1B_u state, than between the 1^1A_g ground state and the 2^1A_g state.

The second approach to V_{ab} is due to Itoh[52] who combined eqs 1 and 3 to obtain

$$\ln(F_b/F_a) = -\Delta E_{ab}/RT - 2 \ln V_{ab} + 2 \ln \Delta E_{ab} \qquad (4)$$

and arrived at $V_{ab} = 140$ cm^{-1} using $1^1B_u/2^1A_g$ fluorescence intensity ratios (estimated by fitting DPH fluorescence spectra with Gaussians[23]) and ΔE_{ab} values in different solvents at room temperature (294 K). This approach lends itself to the evaluation of our results. Because $(x_b/x_a) = (F_b/F_a)$, eq 4 allows the evaluation of V_{ab} by combining the slope and the intercept of the plot of eq 3. The ideal plot in Figure 9 gives $V_{ab} = 182$ cm^{-1}, and with the use of the (x_b/x_a) data in Table 1 for the resolved $2^1A_g/1^1B_u$ spectral mixtures (Figure 8), we obtain $V_{ab} = 198 \pm 12$ cm^{-1}. Within the framework of current theory, we consider the latter value a reliable estimate of V_{ab} and probably the best determination of this quantity to date. The agreement with Itoh's value is reasonable when one considers that his determination of fluorescence intensity ratios neglects the contribution of *s-c*-DPH fluorescence and thus overestimates the contribution of 2^1A_g fluorescence.

Effective Radiative Rate Constants. Our fluorescence quantum yields and lifetimes are in reasonable agreement with previously reported values.[38] They lead to effective radiative constants, k_f^{obs} (Table 2) which, provided that constant polarizability is maintained, increase monotonically with increasing *T*. Because the fluorescence quantum yields and lifetimes are independent of λ_{exc} within experimental uncertainty, we can assume that the increase in k_f^{obs} reflects at least the behavior of the major conformer, *s-t*-DPH. This increase in k_f^{obs} is predicted by the Hudson and Kohler model because the contribution of the strongly allowed 1^1B_u fluorescence will increase with increasing *T*. The model gives

$$k_f^{obs} = k_{fa}\left(\frac{1}{1+K_{ab}}\right) + k_f^{th}\left(\frac{K_{ab}}{1+K_{ab}}\right) \qquad (5)$$

where K_{ab} is the equilibrium constant for $1^1B_u/2^1A_g$ equilibration, and k_f^{th} and k_{fa} are the radiative rate constants of the two states in the same order.[23,52] The contribution of the second term in eq 5 would be negligible if, following common practice, we used $k_f^{th} = n^2 k_{f0}^{th}$, with $k_{f0}^{th} = 2.23 \times 10^8$ s^{-1}, the value calculated by Birks and Dyson[28] with their slightly modified Strickler and Berg relationship.[27] That k_{f0}^{th} value, however, may be seriously underestimated. First, it is much smaller than 3.75×10^8 s^{-1}, the directly measured value for the $1^1B_u \rightarrow 1^1A_g$ transition in isolated *trans*-stilbene,[63] despite the fact that ϵ_{max} in the absorption spectrum of DPH[64] is ca. 2.7 times larger than that of *trans*-stilbene.[65] Adjusting the *trans*-stilbene 3.75×10^8 s^{-1} value by the ϵ_{max} ratio gives $k_{f0}^{th} = 1.0 \times 10^9$ s^{-1} for isolated DPH, which, with $n = 1.402$, corresponds to $k_f^{th} = 2.0 \times 10^9$ s^{-1} under our isopolarizability conditions.[66] Second, substitution of our experimental ΔE_{ab} and V_{ab} values into eq 1 gives $k_f^{th}/k_{fa} = 63$ or 52 for 1445, 182 cm^{-1} (from the ideal plot in Figure 10) or 1431, 198 cm^{-1} (from the plot of the x_a/x_b ratios in Table 1), respectively. These ratios with $k_{fa} = 4.25 \times 10^7$ s^{-1}, based on the lowest k_f^{obs} value in Table 2, give $k_f^{th} = 2.7 \times 10^9$ and 2.2×10^9 s^{-1}. The two independent methods lead to k_f^{th} estimates that are identical within the experimental uncertainty of the measurements, confirming our suspicion that the calculated Birks and Dyson value is too small. Use of the $1^1B_u \rightarrow 1^1A_g$ spectrum in Figure 10 and the DPH absorption spectrum in *n*-octane in the slightly modified Strickler−Berg equation

$$k_f^{th} = \frac{8\pi \cdot c \cdot n_f^3}{N n_a} \langle \tilde{\nu}_f^{-3} \rangle^{-1} \int_0^\infty \frac{\epsilon(\tilde{\nu})}{\tilde{\nu}} \, d\tilde{\nu} = 2.88 \cdot 10^{-9} \frac{n_f^3}{n_a} \langle \tilde{\nu}_f^{-3} \rangle^{-1} \int_0^\infty \frac{\epsilon(\tilde{\nu})}{\tilde{\nu}} \, d\tilde{\nu} \qquad (6)$$

where n_f and n_a, the mean refractive indices in the fluorescence and absorption bands, are assumed equal; *N* is Avogadro's number, *c* is the velocity of light, $\epsilon(\tilde{\nu})$ is the molar absorptivity, and

$$\langle \tilde{\nu}_f^{-3} \rangle^{-1} = \left(\int_0^\infty f(\tilde{\nu}) \, d\tilde{\nu}\right)\left(\int_0^\infty \frac{f(\tilde{\nu})}{\tilde{\nu}^3} \, d\tilde{\nu}\right)^{-1} \qquad (7)$$

where $f(\tilde{\nu})$ is fluorescence intensity, gives $k_f^{th} = 8.83 \times 10^8$ s^{-1}. While larger than the Birks and Dyson value, it is still too small to account for our observations. It is also too small when one considers that the average experimental k_f^{obs} for all-*trans*-1,4-diphenyl-1,3-butadiene in hydrocarbon solvent in the 223−293 K range is 8.8×10^8 s^{-1}.[67] The calculated k_f values in Table 2, based on eq 5 with $k_{fa} = 4.25 \times 10^7$ s^{-1}, $k_f^{th} = 2.0 \times 10^9$ s^{-1}, and $\Delta E_{ab} = 4.1$ kcal/mol, are systematically lower, but reproduce the trend in the experimental values.

Photochemical Implications and Some Puzzles. The possible involvement of the 2^1A_g state in the torsional process leading to a perpendicular intermediate on the S_1 potential energy surface of *trans*-stilbene[68] was postulated by Orlandi and Siebrand (OS),[69] and later extended to the higher members of the α,ω-diphenylpolyene family by Birks.[19,70] Much attention has been focused on this trans ⇄ cis photoisomerization mechanism,[4,14,71] despite early indications that if an A_g state were involved in stilbene photoisomerization,[5,72] it would have to be a higher state than the 2^1A_g state.[73] Nor has anyone offered an explanation of how the trans → cis torsional barrier in S_1 can be created by an A_g/B_u weakly avoided crossing when, on moving from the gas phase[5,63,74] to a hydrocarbon solution,[5,64b,75] its intrinsic magnitude is insensitive to a ca. 5.8 kcal/mol relative stabilization of the 1^1B_u state.[34] The notion of an essentially barrierless torsional motion in the 2^1A_g state of all-*trans*-DPH was dispelled by our observation of very low photoisomerization quantum yields that are governed by photoisomerization activation energies that are considerably higher than the effective ΔE_{ab} values.[43,76]

Our interpretation of the fluorescence spectra of DPH leads to several remarkable coincidences: (i) Fluorescence quantum yields are insensitive to the increase in *T* under isopolarizability conditions, probably due, in part, to a nearly exact compensation of parallel increases in the isomerization rate constants and the effective radiative rate constants of *s-t*-DPH. (ii) Fluorescence lifetimes are monoexponential, solvent specific, and insensitive to changes in *T* in each of several saturated hydrocarbon

solvents. This finding, reported by Cehelnik et al. for DPH in 3-methylpentane, *n*-hexane, *n*-heptane, and methylcyclohexane,[38] was confirmed by us for the *n*-alkanes used in this work (this includes C_{12}, Table 3, for which others[55] have claimed a small increase of τ_f with increasing *T*). Apparently, the fluorescence lifetimes of *s-cis*- and *s-trans*-DPH conformers are identical in each solvent and are not affected by changes in *T*. (iii) We have not detected a second, minor, shorter-lived component that has been reported in some solvents. Consistent with the conclusion in (ii), fluorescence lifetimes and quantum yields are λ_{exc}-independent in each of the alkanes (see, e.g;, Table 3). In the case of *s-t*-DPH, we can postulate that the expected increase in ΔE_{ab} with increasing *T* causes a net loss in the Boltzmann population of the 1^1B_u state, leading to a decrease in the effective radiative rate constant, which is exactly compensated by the concomitant increase in the photoisomerization rate. This would account for the decrease in the fluorescence quantum yield with increasing *T* in a specific alkane (see Table 3 and the relative areas of the fluorescence spectra in Figure 1; in C_8, ϕ_f^{obs} decreases from 0.71 at 293.2 K to 0.41 at 353.2 K), while a constant lifetime is coincidentally maintained. We can advance no such explanation (convoluted as it may be) to account for the parallel lifetime behavior of the s-cis conformer. However, in view of its long fluorescence lifetime and small effective radiative rate constant, the fluorescence of *s-c*-DPH also appears to correspond to a forbidden radiative transition.

It is important to keep in mind that most of the radiationless decay in singlet excited DPH in most solvents is photochemically unproductive and, at least in acetonitrile, *T*-independent.[43] The complementarity between radiative and photoisomerization decay pathways, experimentally demonstrated by Fischer and co-workers and confirmed by Yoshihara and co-workers for *trans*-stilbene,[77−79] does not apply to the butadiene[80] and hexatriene[76] members of the α,ω-diphenylpolyene family. The common practice of assigning all radiationless decay competing with fluorescence in the higher α,ω-diphenylpolyenes and related molecules (see, e.g., ref 19) to photoisomerization pathways is imprudent and should be avoided.

Acknowledgment. The National Science Foundation, most recently by grant CHE 0314784, supported this research. J.S. dedicates this paper to the memory of Bryan E. Kohler with appreciation for his encouragement to work in this area.

Supporting Information Available: Total energies and Cartesian coordinates for the DPH stationary points optimized at the B3LYP/6-311+G(d,p). This material is available free of charge via the Internet at http://pubs.acs.org.

References and Notes

(1) Presented in part at the Pacifichem 2000 (Joint Meeting of the American, Canadian, Japanese, and Korean Chemical Societies) Honolulu, Hawaii, December, 2000.

(2) Hudson, B. S.; Kohler, B. E. *Annu. Rev. Phys. Chem.* **1974**, *25*, 437−460.

(3) Hudson, B. S.; Kohler, B. E.; Schulten, K. In *Excited States*; Lim, E. C., Ed.; Academic Press: New York, 1982; Vol. 6, pp 1−95.

(4) (a) Allen, M. T.; Whitten, D. G. *Chem. Rev.* **1989**, *89*, 1691−1702. (b) Whitten, D. G. *Acc. Chem. Res.* **1993**, *26*, 502−509.

(5) Saltiel, J.; Sun, Y.-P. *Photochromism, Molecules and Systems*; Dürr, H., Bouas-Laurent, H., Eds.; Elsevier: Amsterdam, 1990; pp 64−164.

(6) Hudson, B. S.; Kohler, B. E. *Chem. Phys. Lett.* **1972**, *14*, 299−304.

(7) Shulten, K.; Karplus, M. *Chem. Phys. Lett.* **1972**, *14*, 305−309.

(8) See also (a) Tavan, P.; Schulten, K. *J. Chem. Phys.* **1979**, *70*, 5407−5413. (b) Orlandi, G.; Zerbetto, F.; Zgierski, M. Z. *Chem. Rev.* **1991**, *91*, 867−891.

(9) Hsu, C.-P.; Hirata, S.; Head-Gordon, M. *J. Phys. Chem. A* **2001**, *105*, 451−458.

(10) Catalan, J.; de Paz, J. L. G. *J. Chem. Phys.* **2004**, *120* 1864−1872.

(11) Catalan, J. *J. Chem. Phys.* **2003**, *119*, 1373−1385.

(12) Maitra, N. T.; Zhang, F.; Cave, R. J.; Burke, K. *J. Chem. Phys.* **2004**, *120*, 5932−5937.

(13) Cave, R. J.; Zhang, F.; Maitra, N. T.; Burke, K. *Chem. Phys. Lett.* **2004**, *389*, 39−42.

(14) Kohler, B. E. *Chem. Rev.* **1993**, *93*, 41−54.

(15) Kohler, B. E.; Spiglanin, T. A. *J. Chem. Phys.* **1984**, *80*, 5465−5471.

(16) Kohler, B. E.; Spiglanin, T. A. *J. Chem. Phys.* **1985**, *82*, 2939−2941.

(17) Fang, H. L.-B.; Thrash, R. J.; Leroi, G. E. *Chem. Phys. Lett.* **1978**, *57*, 59.

(18) Andrews, J. R.; Hudson, B. S. *J. Chem. Phys.* **1978**, *68*, 4587−4594.

(19) Birks, J. B.; Tripathi, G. N. R.; Lumb, M. D. *Chem. Phys.* **1978**, *33*, 185−194.

(20) (a) Pfeiffer, M.; Werneke, W.; Hogiu, S.; Kummrow, A.; Lau, A. *Chem. Phys. Lett.* **1998**, *295*, 56−62. (b) Hogiu, S.; Werneke, W.; Pfeiffer, M.; Lau, A. *Chem. Phys. Lett.* **1999**, *303*, 218−222. (c) Werneke, W.; Hogiu, S.; Pfeiffer, M.; Lau, A.; Kummrow, A. *J. Phys. Chem. A* **2000**, *104*, 4211−4217.

(21) Alford, P. C.; Palmer, T. F. *Chem. Phys. Lett.* **1982**, *86*, 248−253.

(22) Alford, P. C.; Palmer, T. F. *J. Chem. Soc., Faraday Trans. 2* **1983**, *79*, 433−447.

(23) Itoh, T.; Kohler, B. E. *J. Phys. Chem.* **1987**, *91*, 1760−1764.

(24) Hilinski, E. F.; McGowan, W. M.; Sears, D. F., Jr.; Saltiel, J. *J. Phys. Chem.* **1996**, *100*, 3308−3311.

(25) Yee, W. A.; O'Neil, R. H.; Lewis, J. W.; Zhang, J. Z.; Kliger, D. S. *Chem. Phys. Lett.* **1997**, *276*, 430−434.

(26) Hogiu, S.; Werneke, W.; Pfeiffer, M.; Lau, A.; Steinke, T. *Chem. Phys. Lett.* **1998**, *287*, 8−16.

(27) Strickler, S. J.; Berg, R. A. *J. Chem. Phys.* **1962**, *37*, 814−822.

(28) Birks, J. B.; Dyson, D. J. *Proc. R. Soc. London, Ser. A* **1963**, *275*, 135−148.

(29) Saltiel, J.; Sears, D. F., Jr.; Sun, Y.-P.; Choi, J.-O. *J. Am. Chem. Soc.* **1992**, *114*, 3607−3612.

(30) Jacobs, H. J. C.; Havinga, E. *Adv. Photochem.* **1979**, *11*, 305−373.

(31) Saltiel, J.; Sears, D. F., Jr.; Turek, A. M. *J. Phys. Chem. A* **2001**, *105*, 7569−7578.

(32) Saltiel, J.; Choi, J.-O.; Sears, D. F., Jr.; Eaker, D. W.; Mallory, F. B.; Mallory, C. W. *J. Phys. Chem.* **1994**, *98*, 13162−13170.

(33) Basu, S. *Adv. Quantum Chem.* **1964**, *1*, 145.

(34) Sklar, L. A.; Hudson, B. S.; Petersen, M.; Diamond, J. *Biochemistry* **1977**, *16*, 813−818.

(35) Brey, L. A.; Schuster, G. B.; Drickamer, H. G. *J. Chem. Phys.* **1979**, *71*, 2765−2772.

(36) Suppan, P.; Ghoneim, N. In *Solvatochromism*; The Royal Society of Chemistry: Cambridge, U.K., 1997.

(37) Cehelnik, E. D.; Cundall, R. B.; Lockwood, J. R.; Palmer, T. *Chem. Phys. Lett.* **1974**, *27*, 586−588.

(38) Cehelnik, E. D.; Cundall, R. B.; Lockwood, J. R.; Palmer, T. *J. Phys. Chem.* **1975**, *79*, 1369−1376.

(39) Jones, G. R.; Cundall, R. B. *Chem. Phys. Lett.* **1986**, *126*, 129−133.

(40) Saltiel, J.; Sears, D. F., Jr.; Choi, J.-O.; Sun, Y.-P.; Eaker, D. W. *J. Phys. Chem.* **1994**, *98*, 35−46.

(41) Melhuish, W. H. *J. Phys. Chem.* **1961**, *65*, 229−235.

(42) Meech, S. R.; Phillips, D. *J. Photochem.* **1983**, *23*, 193−217.

(43) Saltiel, J.; Krishnamoorthy, G.; Huang, Z.; Ko, D.-H.; Wang, S. *J. Phys. Chem. A* **2003**, *107*, 3178−3186.

(44) Frisch, M. J.; Trucks, G. W.; Schlegel, H. B.; Scuseria, G. E.; Robb, M. A.; Cheeseman, J. R.; Zakrzewski, V. G.; Montgomery, J. A., Jr.; Stratmann, R. E.; Burant, J. C.; Dapprich, S.; Millam, J. M.; Daniels, A. D.; Kudin, K. N.; Strain, M. C.; Farkas, O.; Tomasi, J.; Barone, V.; Cossi, M.; Cammi, R.; Mennucci, B.; Pomelli, C.; Adamo, C.; Clifford, S.; Ochterski, J.; Petersson, G. A.; Ayala, P. Y.; Cui, Q.; Morokuma, K.; Malick, D. K.; Rabuck, A. D.; Raghavachari, K.; Foresman, J. B.; Cioslowski, J.; Ortiz, J. V.; Stefanov, B. B.; Liu, G.; Liashenko, A.; Piskorz, P.; Komaromi, I.; Gomperts, R.; Martin, R. L.; Fox, D. J.; Keith, T.; Al-Laham, M. A.; Peng, C. Y.; Nanayakkara, A.; Gonzalez, C.; Challacombe, M.; Gill, P. M. W.; Johnson, B. G.; Chen, W.; Wong, M. W.; Andres, J. L.; Head-Gordon, M.; Replogle, E. S.; Pople, J. A. *Gaussian 98*, revision A.7; Gaussian, Inc.: Pittsburgh, PA, 1998.

(45) (a) Schlegel, H. B. *J. Comput. Chem.* **1982**, *3*, 214−218. (b) Schlegel, H. B. *Adv. Chem. Phys.* **1987**, *67*, 249. (c) Schlegel, H. B. In *Modern Electronic Structure Theory*; Yarkony, D. R., Ed.; World Scientific: Singapore, 1995; p 459.

(46) (a) Becke, A. D. *Phys. Rev. A* **1988**, *38*, 3098−3100. (b) Lee, C.; Yang, W.; Parr, R. G. *Phys. Rev. B* **1988**, *37*, 785−789.

(47) (a) Becke, A. D. *J. Chem. Phys.* **1993**, *98*, 5648−5652. (b) Stevens, P. J.; Devlin, F. J.; Chabalowski, C. F.; Frisch, M. J. *J. Phys. Chem.* **1994**, *98*, 11623−11627.

(48) Turek, A. M.; Krishnamoorthy, G.; Phipps, K.; Saltiel, J. *J. Phys. Chem. A* **2002**, *106*, 6044−6052.

(49) Sun, Y.-P.; Sears, D. F., Jr.; Saltiel, J. *J. Am. Chem. Soc.* **1988**, *110*, 6277−6279.

(50) Sun, Y.-P.; Sears, D. F., Jr.; Saltiel, J. *J. Am. Chem. Soc.* **1989**, *111*, 706−711.

(51) (a) Lawton, W. H.; Sylvestre, E. A. *Technometrics* **1971**, *13*, 617−633. (b) Sylvestre, E. A.; Lawton, W. H.; Maggio, M. S. *Technometrics* **1974**, *16*, 353−368.

(52) Itoh, T. *Chem. Phys. Lett.* **1989**, *159*, 263−266.

(53) Levshin, V. L. *Z. Phys.* **1931**, *72*, 368, 382.

(54) For a recent review of polyene photophysics, see Fuss, W.; Haas, Y.; Zilberg, S. *Chem. Phys*. **2000**, *259*, 273−295.

(55) See, for example, Parasassi, T.; De Stacio, G.; Rusch, R. M.; Gratton, E. *Biophys. J*. **1991**, *59*, 466−475. For recent refs, see (a) Hammer, K. A.; Carson, C. F.; Riley, T. V. *J. Antimicrob. Chemother*. **2004**, *53*, 1081−1085. (b) Pandey, B. N.; Mishra, K. P. *J. Biochem., Mol. Biol. Biophys.* **2002**, *6*, 267−272. (c) Marathe, D.; Mishra, K. P. *Radiat. Res.* **2002**, *157*, 685−692. (d) Asamoto, Y.; Tazuma, S.; Ochi, H.; Chayama, K.; Suzuki, H. *Biochem. J.* **2001**, *359*, 605−610.

(56) Spalletti, A.; Bartocci, G.; Masetti, F.; Mazzucato, U.; Cruciani, G. *Chem. Phys.* **1992**, *160*, 131−144.

(57) Saltiel, J.; Zhang, Y.; Sears, D. F., Jr. *J. Phys. Chem.* **1997**, *101*, 7053−7060.

(58) Chattopadhyay, S. K.; Das, P. K.; Hug, G. L. *J. Am. Chem. Soc.* **1982**, *104*, 4507−4514.

(59) Mateo, C. R.; Lillo, M. P.; Brochon, J. C.; Martínez-Ripoll, M.; Sanz-Aparicio, J.; Acuña, A. U. *J. Phys. Chem.* **1993**, *97*, 3486−3491.

(60) Hudson, B. S.; Kohler, B. E. *J. Chem. Phys.* **1973**, *59*, 4984−5002.

(61) Alford, P. C.; Palmer, T. F. P. *Chem. Phys. Lett.* **1986**, *27*, 19−25.

(62) Bondarev, S. L.; Bachilo, S. M. *J. Photochem. Photobiol. A: Chem.* **1991**, *59*, 273−283.

(63) (a) Syage, J. A.; Lambert, W. R.; Felker, P. M.; Zewail, A. H.; Hochstrasser, R. M. *Chem. Phys. Lett.* **1982**, *88*, 266. (b) Syage, J. A.; Felker, P. M.; Zewail, A. H. *J. Chem. Phys.* **1984**, *81*, 4706. (c) Felker, P. M.; Zewail, A. H. *J. Phys. Chem.* **1985**, *89*, 5402.

(64) Lunde, K.; Zechmeister, L. *J. Am. Chem. Soc.* **1954**, *76*, 2308−2313.

(65) (a) Marinari, A.; Saltiel, J. *Mol. Photochem.* **1976**, *7*, 225−249. (b) Saltiel, J.; Waller, A. S.; Sears, D. F., Jr.; Garrett, C. Z. *J. Phys. Chem.* **1993**, *97*, 2516−2522.

(66) Turro, N. J. *Modern Molecular Photochemistry*; Benjamin/Cummings: Menlo Park, CA, 1978; p 90.

(67) Birch, D. J. S.; Imhof, R. E. *Chem. Phys. Lett*. **1982**, *88*, 243−247.

(68) (a) Saltiel, J. *J. Am. Chem. Soc*. **1967**, *89*, 1036−1037. (b) Saltiel, J. *J. Am. Chem. Soc.* **1968**, *90*, 6394−6400.

(69) Orlandi, G.; Siebrand, W. *Chem. Phys. Lett.* **1974**, *30*, 352−354.

(70) (a) Birks, J. B.; Birch, D. J. S. *Chem. Phys. Lett.* **1975**, *31*, 608−610. (b) Birks, J. B. *Chem. Phys. Lett*. **1978**, *54*, 430−434.

(71) Waldeck, D. H. *Chem. Rev.* **1991**, *91*, 415−436.

(72) Troe, J.; Weitzel, K. M. *J. Chem. Phys.* **1988**, *88*, 7030.

(73) (a) Orlandi, G.; Palmieri, P.; Poggi, G. *J. Am. Chem. Soc.* **1979**, *101*, 3492−3497. (b) Fuke, K.; Sakamoto, S.; Ueda, M.; Itoh, M. *Chem. Phys. Lett*. **1980**, *74*, 546−548. (c) Hohlneicher, G.; Dick, B. *J. Photochem.* **1984**, *27*, 215.

(74) Majors, T. J.; Even, U.; Jortner, J. *J. Chem. Phys.* **1984**, *81*, 2330 and other papers in this series.

(75) (a) Saltiel, J.; Sun, Y.-P. *J. Phys. Chem.* **1989**, *93*, 6246−6250. (b) Sun, Y.-P.; Saltiel, J. *J. Phys. Chem*. **1989**, *93*, 8310−8316.

(76) (a) Saltiel, J.; Ko, D.-H.; Fleming, S. A. *J. Am. Chem. Soc.* **1994**, *116*, 4099−4100. (b) Saltiel, J.; Wang, S.; Watkins, L. P.; Ko, D.-H. *J. Phys. Chem. A* **2000**, *104*, 11443−11450.

(77) (a) Charlton, J. L.; Saltiel, J. *J. Phys. Chem.* **1977**, *81*, 1940−1944. (b) Saltiel, J.; Charlton, J. L. In *Rearrangements in Ground and Excited States*; de Mayo, P., Ed.; Academic Press: New York, 1980; Vol. III, pp 25−89.

(78) (a) Malkin, S.; Fischer, E. *J. Phys. Chem.* **1964**, *68*, 1153−1163. (b) Sharafi, S.; Muszkat, K. A. *J. Am. Chem. Soc.* **1971**, *93*, 4119−4125.

(79) Sumitani, M.; Nakashima, N.; Yoshihara, K.; Nagakura, S. *Chem. Phys. Lett*. **1977**, *51*, 183−185.

(80) Yee, W. A.; Hug, S. J.; Kliger, D. S. *J. Am. Chem. Soc*. **1988**, *110*, 2164−2169.